AERODYNAMICS ASSESSMENT USING CFD FOR A LOW DRAG SHELL ECO-MARATHON CAR

E. Abo-Serie [1,*], E. Oran[2], O Utcu[3]

ABSTRACT

Having a small car running with low power can be achieved by reducing the aerodynamics drag, rolling resistance and mechanical frictions between the moving parts. The Shell Eco-Marathon competition held around the world with events in Europe, USA and Asia shows every year new techniques and ideas to reduce the power needed to drive the car. The record of over 3400 km on the equivalent of a single litre of fuel is an indication of how car can run efficiently. The problem with these low drag cars is the driver perception about the shape of the car. Although the tear drop shape is known as having the minimum drag, practically this shape cannot be used due to size and packaging limitations in addition to the safety issue. In this work, a low drag concept car is proposed using initial CAD design. The concept car is examined using a commercial CFD software by simulating the airflow around car. The spatial distribution of the pressure and velocity vectors are utilized to improve the car shape and to achieve a low drag force coefficient while keeping the down force at its minimum value. By changing the car front, underneath and rear shapes, it was possible to reduce the drag coefficient from 0.430 for the baseline to 0.127 for the final design, while meeting the competition regulations

INTRODUCTION

It is expected that the future of urban mobility may change radically due to the increase in world populations and the rapid growth of energy request in addition to the unsustainable environmental pollution levels. As more people emigrating from rural areas to city as more congestion and emissions are generated in the cities. With such conditions, it became viable to use an electric car in heavily populated areas. However, the car design and shape still heavy with weight ranging 1000-1500 kg which lead to more energy consumption. The response to that is to be able to design lighter, low cost and low drag cars. In that trend was the Shell Eco-Marathon competition. In this competition, the main aim is to have a car that can be driven longer distance with an equivalent energy of 1 liter of gasoline. Many international car manufacturers are keen to be involved in this competition as new technologies and ideas are emerging [1].

As the weight of the car is playing a main role in reducing the rolling resistance and friction losses between the moving parts, the aerodynamics force particularly the drag force is also a major factor. In passenger cars, the aerodynamics force exceeds the rolling resistance force as the car speed exceeds approximately 35 km/hr [2]. The aerodynamics force is theoretically directly proportional to the square to the car speed. It is therefore important to have the car body streamlined to effectively decrease the coefficient of drag [3]. Although the tear-drop shape is well known to be the most efficient shape for minimum drag force, it is practically not feasible due to its longer length [4]. Nevertheless, having a shape similar to the tear-drop while chopping its end can still achieve stream airflow with small drag loss. The tear drop shape car was not acceptable in the past but perception of people about the shape of the car is now slowly changing as many cars start to appear in the market more streamlines and receives customer satisfactions.

To be able to reduce the flow losses and the drag force on the ground vehicle, the effect of the flow on each part of the vehicle has to be studied. Computational Fluid Dynamics, CFD, allows engineers to examine the airflow characteristics over a vehicle as a whole, and thus determine overall aerodynamic loads, or local flows such as those through cooling intakes, when changing the vehicle geometry. Due to the accuracy and economy of using CFD, it is not only used by automotive industry to study the car external body shape. It is also employed in mapping airflow through the heat exchangers (e.g. radiators, condensers, etc.), engine bay, and even inside the car cabinet to ensure adequate cooling flow and a comfortable thermal environment for the vehicle occupants [5].

Geometrical modifications, through topology optimization, can improve the flow around the car and reduce the flow vortices and assist in achieving vehicle stability. Nevertheless, it is not the only option of improving the fluid dynamic performance of the car. Recently there is a growing interest in qualifying active flow control devices for vehicle aerodynamics using blowing air or using continuous or oscillating jet [6,7,8]. With the development of the CFD for flow simulation, it became a standard tool in industry to develop the car shape before having the car tested in a wind tunnel and it is commonly used by Shell Eco-marathon teams [9,10]. However, attention has to be paid to the gird size independency [11].

In most racing car competitions, a trade-off between the drag force and downforce (negative lift) has to be carried out for each specific racing track. This is the case since competitions are usually racing on time. Nevertheless, Shell Eco-Marathon is not racing on time but on minimum fuel consumption. It is therefore not important to have high downforce to have the car moving fast in the corners. Increasing the downforce is known to be associated by an increase in the drag force [4]. The main concern, therefore, is achieving as minimum drag as possible while keeping slight negative lift to ensure the car stability.

In this study, CFD analysis has been employed to inspect the airflow distribution around a small car, which was designed to contribute in the Shell Eco-Marathon competition using the commercial software, STARCCM+. The tear drop shape was adopted as ideal case and then modified to comply with the Shell Eco-Marathon regulation and the packaging requirements.

AERODYNAMIC DRAG

Aerodynamic drag is defined as the axial or longitudinal force resulting from air flowing past the vehicle body as shown in Figure 1. It represents the forces that resist the car to move forward. The two components, pressure drag and skin friction, account for the aerodynamic drag of a vehicle. An alternative representation of the drag is as the momentum loss of the air in the vehicle wake, along with the rotational energy imparted to this air by end vortices and other vorticity generated by the vehicle. The drag can be divided into components related to the various regions and parts of the vehicle; fore-end of the car and rear of the car pressure drag, wheel drag, cooling drag, underbody drag, protuberance drag and the skin friction on the upper body surface. The pressure drag at rear of the car is dictated by the extent to which pressure can be recovered at the rear of the car body.
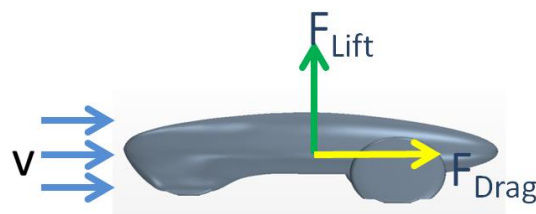

Figure 1. Drag and lift force directions

COEFFICIENTS OF DRAG

The drag coefficient can be calculated from equation 1[12].

$$C_d = \frac{F_d}{0.5 \rho v^2 A} \tag{1}$$

where, F_d is the drag force, $\square$ is the free stream air density, v being the free stream air velocity, and A is the projected frontal cross sectional area of the car.

The drag force represents the aerodynamics force that resists the car to move forward. This force is the surface integral of the pressure and shear force components in the direction of the car motion. The drag force can either experimentally measured such as in case of wind tunnel measurements or calculated such as in case of using CFD.

MATHEMATICAL MODEL

The airflow distributions around the car are identified by solving the fluid flow governing equations using the Eulerian approach. In this study, the Reynolds Averaged Navier Stokes (RANS) equations are solver together with the continuity equation. Steady isothermal flow is assumed. Since the Mach number is very small, the change in air density due to the variation is airflow is negligible and therefore incompressible flow is also assumed. The turbulent k-ε model is implemented to estimate the Reynolds stress terms appeared from averaging the momentum equations. The equations employed in the model are as follow:

Continuity Equation

$$\frac{\partial}{\partial x_i}\left(\rho u_i\right) = 0 \tag{2}$$

Where ρ represents the density (kg/m³), u the velocity (m/s),

Reynolds Averaged Navier Stokes (Momentum) Equations

$$\left.\begin{aligned}
\frac{\partial}{\partial x_j}\left(\rho u_i u_j\right) &= -\frac{\partial P}{\partial x_i} \\
&+ \frac{\partial}{\partial x_j}\left[\mu\left(\frac{\partial u_i}{\partial x_j} + \frac{\partial u_j}{\partial x_i} - \frac{2}{3}\delta_{ij}\frac{\partial u_m}{\partial x_m}\right)\right] \\
&+ \frac{\partial}{\partial x_j}\left[\mu_t\left(\frac{\partial u_i}{\partial x_j} + \frac{\partial u_j}{\partial x_i}\right) - \frac{2}{3}\left(\rho k + \mu_t\frac{\partial u_m}{\partial x_m}\right)\delta_{ij}\right]
\end{aligned}\right\} \tag{3}$$

Where ρ represents the air density (kg/m³), u the velocity (m/s), P the pressure (Pa), k the turbulence kinetic energy (m²/s²), μ the laminar viscosity (kg/m s), and μt the turbulent viscosity (kg/ms), the subscripts: i, j and m represent the directions (x, y, and z). δ_{ij} is the Kronecker delta, it is 1 when i = j, otherwise it is 0.

Turbulence Equations

$$\left.\begin{aligned}
\frac{\partial}{\partial x_i}\left(\rho k u_i\right) &= \frac{\partial}{\partial x_j}\left[\left(\mu + \frac{\mu_t}{\sigma_k}\right)\frac{\partial k}{\partial x_j}\right] + G_k - \rho\varepsilon - Y_M \\
\frac{\partial}{\partial x_i}\left(\rho\varepsilon u_i\right) &= \frac{\partial}{\partial x_j}\left[\left(\mu + \frac{\mu_t}{\sigma_\varepsilon}\right)\frac{\partial\varepsilon}{\partial x_j}\right] + C_{1\varepsilon}\frac{\varepsilon}{k}G_k - C_{2\varepsilon}\rho\frac{\varepsilon^2}{k}
\end{aligned}\right\} \tag{4}$$

where σ_k and σ_ε are the turbulent Prandtl numbers for k and ε, and constant values of 1.0 and 1.3 are used, respectively. G_k (kg/m s³) represents the generation of turbulence kinetic energy due to the mean velocity gradients, and YM (kg/m s³) is the contribution of the fluctuating dilatation in turbulence to the overall dissipation rate, they are calculated as

$$
\left.
\begin{aligned}
G_K &= \left[\mu_t \left(\frac{\partial u_i}{\partial x_j} + \frac{\partial u_j}{\partial u_i} \right) - \frac{2}{3} \left(\rho k + \mu_t \frac{\partial u_m}{\partial x_m} \right) \delta_{ij} \right] \frac{\partial u_j}{\partial xi} \\
Y_M &= 2\rho\varepsilon \frac{k}{\gamma RT} \\
\gamma &= \frac{c_P}{c_v}
\end{aligned}
\right\} \tag{5}
$$

Y_M is the contribution of the fluctuating dilatation to the dissipation rate (kg/m s^3), is the specific heat ratio and, the eddy viscosity, μ_t is calculated as:

$$
\mu_t = \rho C_\mu \frac{k^2}{\varepsilon} \tag{6}
$$

Where σ_k and σ_ε are the turbulent Prandtl numbers for k and ε, and constant values of 1.0 and 1.3 are used, respectively. The values of the model constants $C_{1\varepsilon}$, $C_{2\varepsilon}$ and C_μ are 1.44, 1.92 and 0.09, respectively.

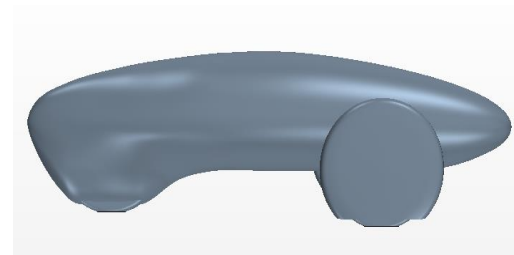## MODEL PREPARATION AND MESHING

Different CADs have been examined until reaching the best design. Figure 2 shows the first baseline and an intermediate and the final CAD designs. The CAD surface is then imported into STARCCM+ for further analysis.
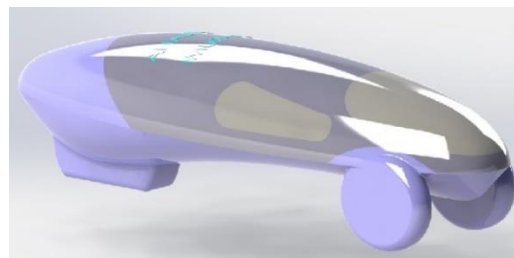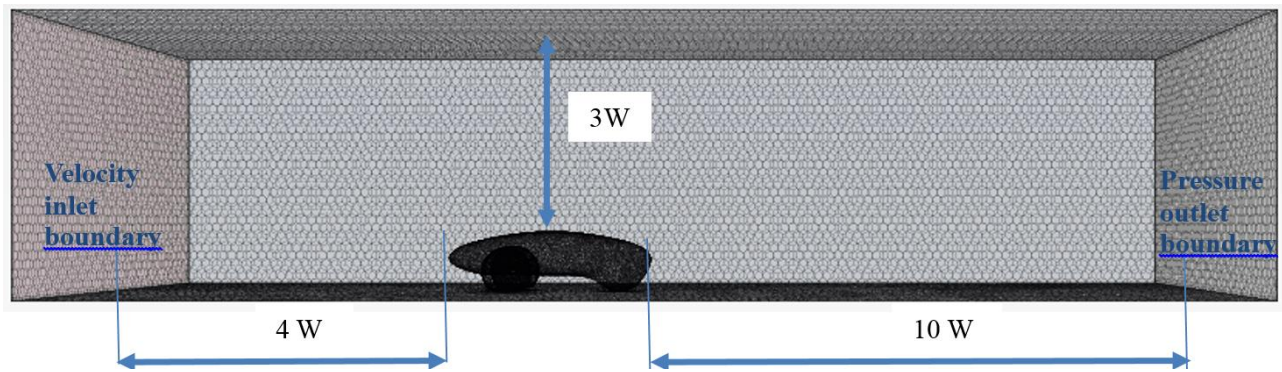

a)   Baseline design
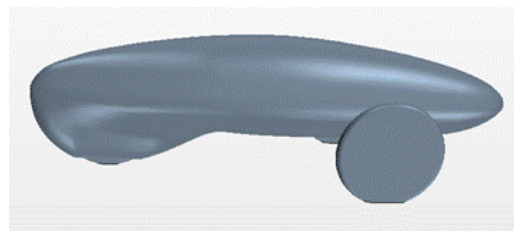
b)   Intermediate design

c)   Final design

Figure 2. Sample of the car CAD designs

Figure 3. Computation domain size and boundary conditions

Having the car imported into STARCCM+, a wind tunnel wall has then been constructed and the car is located inside with a yaw angle zero. The airflow domain has a length of 10 times the car width downstream the car and 6 times in front of the car. To minimize the blockage effect, a distance 3 times the car height is allowed above and on the two sides of the car. The blockage ratio which is defined as the frontal projection area of the car to the cross sectional area of the tunnel is found to be less than 5%. It is worth mentioning that this blockage ratio leads to the drag coefficient to be overestimated. According to previous work on a model of Fiat Linea car the drag coefficient was overestimated by 9.2 % for a blockage ratio of 5 % [13].

Figure 3 shows the computation domain and the boundary conditions. Inlet velocity boundary conditions of 25 km/h (7.3 m/s) is applied for the air entering the domain and an outlet pressure boundary conditions is assumed at the exit surface of the domain. Other surfaces including the car are considered as fixed walls and all y+ wall function is used. The effect of rotating wheel has been neglected in this study.

A polyhedral mesh is applied to the airflow domain as it can easily fit with different geometry. Meshing is an important part of a CFD set up in order to capture the flow details. The finer the mesh, the more accuracy the result is. The downside of fine mesh is the increase in computational time, therefore, the right balance between computation time and accuracy is needed to identify the mesh size. Very fine mesh may also lead to round off error. Two regions within the computation domain are defined to allow for custom mesh to be applied. The region closer to the car is refined by setting the mesh size to 30 % of the main mesh size since the velocity gradient is much larger in that region. Volume control mesh has not been used based on recommendations of previous study which showed it is computationally expensive and not achieving much difference in drag coefficient value (less than 1%). Prism Layer Mesher is also applied to the surface of the car to accurately calculate the shear force. The first cell size attached to the car has been chosen to keep the boundary layer within the logarithmic law by keeping Y+ value less than of 100.

MESH INDEPENDENT STUDY

To ensure that the mesh size has minimum effect on the final results, a mesh independent study has been carried out. The number of volume cells are changed in two different runs 659,336, 683,177. A third run with a very fine mesh of 2,420,218 cells is hen carried out. The drag coefficient for each run has been calculated based on integrating the pressure and shear force over the car surface and the results has been listed in Table 1. Reducing the mesh size does reduce the drag coefficient but the effect is not significant 2.2 %. It was therefore enough to continue the simulation with a mesh size of 683,177 cells. Figure 4 shows the flow domain with mesh for two sizes. The sizes of the cells are scaled by the same factor.

Table 1. The effect of mesh size on drag coefficient

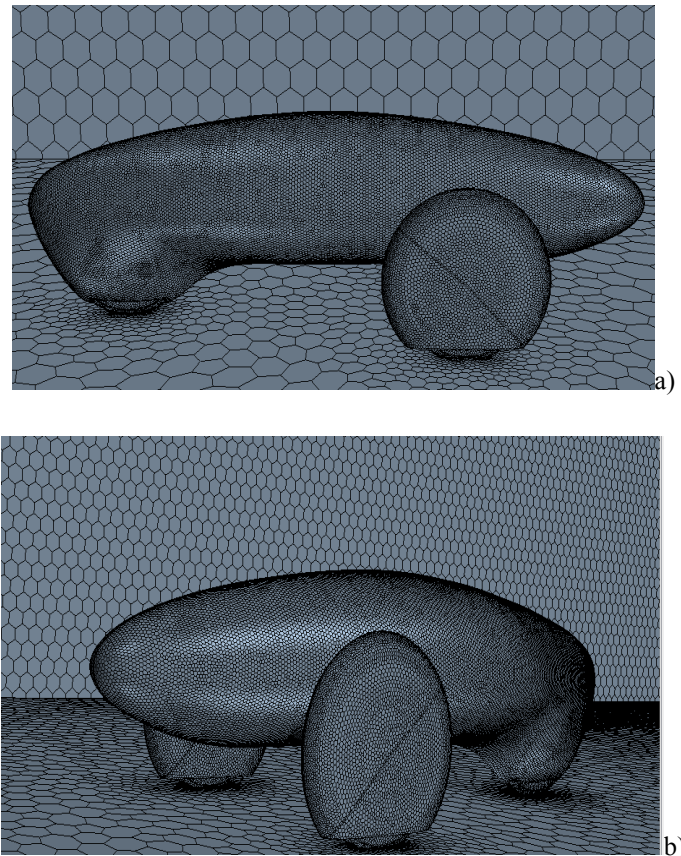|	Number of cells	Number of iterations	Drag coefficients
Run-1	659,336	1000	0.1283
Run-2	683,177	1000	0.1272
Run-3	2.420,218	1000	0.1255

Figure 4. Flow domain with two mesh sizes

RESULTS AND DISCUSSION

Before examining the results, the simulation was run to 1000 iterations which was enough to reach steady state conditions and the residual reach a value at least 5x10-5 as shown in Figure 5. This is generally enough for the balance of the conservations equations in such application.

Although the baseline was visualized from a low drag and try to replicate that shape with a cover wheel, The CFD results showed a large flow separation in different regions. The calculated drag coefficient was found to be 0.43 which is larger than the acceptable level for many recent sedan or hatchback cars currently available in the market. It is a fact that any change in the shape of the car affects the whole flow domain. Therefore, a small change in the car shape has to be carried out at a time and to be able to observe the effect on the flow at different parts of the car. This iterative method was carefully executed to reach the final design with a drag coefficient of 0.127. There are some optimization methods such Genetic Algorithms, Evolution Strategies or Adaptive Hybrid Methods [14] and more recently using Neural Network [15]. These methods can automatically adapt the car shape to achieve a minimum drag, nevertheless all these methods have their limitations and need specific geometrical parameters for the optimization process to work.

Figure 6 shows the velocity vector on a symmetric longitudinal plane around the baseline car. Different areas that need improvements can be observed. At the rear of the car, flow separation occurs and the associated recirculation zone size need to be reduced to lower the drag. The second noticeable area is underneath frontal part of the car which has high velocity of the airflow. This is attributed to the diffuser effect as a result of the convex shape of the car floor relative to the ground. The high velocity underneath the frontal part of the car not only raises an issue about car stability but also results in higher drag due to flow restriction by the rear car wheel cover.

To understand the flow structure the pressure distribution on the car surface and on the same longitudinal plane is plotted in Figure 7. The high pressure area at the nose of the car front seems to also affect in a larger area. Underneath the car is also clearly appear with high air pressure zone in facing the rear wheel cover. The effect of rear flow separation zone on the pressure distribution is also shown.
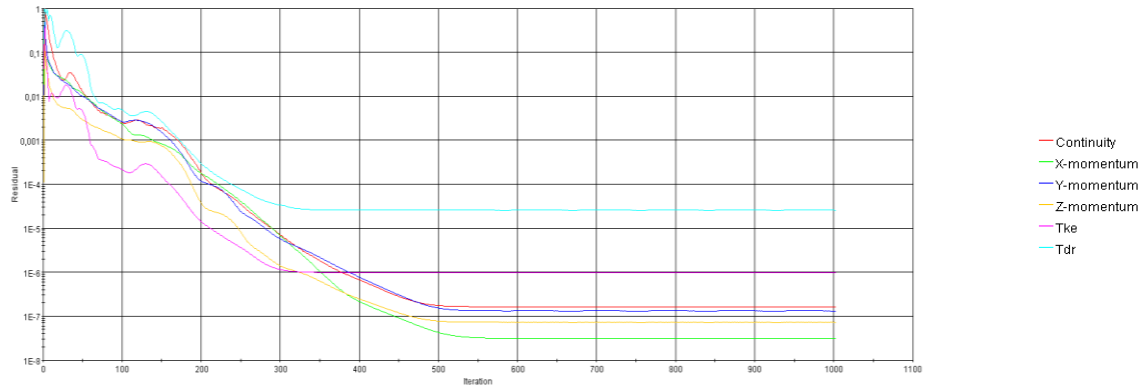
Figure 5. The residual of the conservation equations as applied on the domain for 1000 iterations
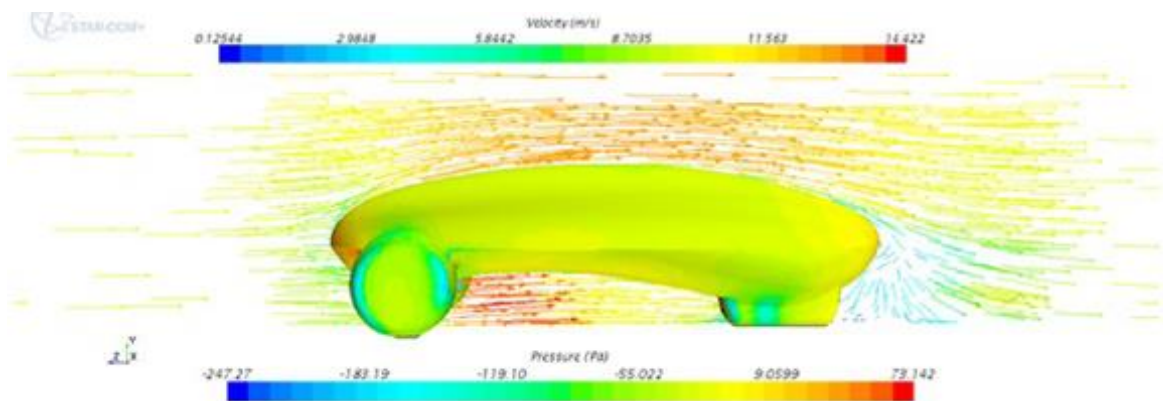

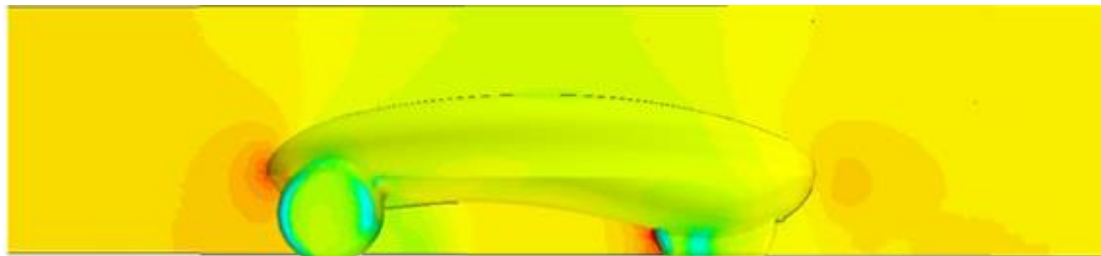**Figure 6.** Velocity vector of the baseline design

**Figure 7.** Pressure distribution on the car surface and on a longitudinal plane.

To improve the baseline car shape, the frontal nose of the car is moved forward away from the frontal wheel and has been sloped. The second modification was made to underneath the car by changing the convex to concave shape. The third modification was related to the rear of the car which has been modified from almost circular end shape to a 30° angle shape while smoothing the rear wheel cover shape with the car rear body, as shown in Figure 2c.

Figure 8 shows the velocity vector of the final design after applying the above mentioned modifications. The obvious notice is that the flow velocity underneath the car is still high but now, it is uniform along the car length. This is not bad as it balances the pressure located above the car and therefore allow the can to have a downforce which stabilizes the car. The second observation is the flow at the rear of the car, the airflow admitted from underneath the car is smoothly attached to the car body and joining the main airflow stream eliminating the flow separation zone. The flow did not show any separation throughout the car body. At the rear, the flow was smoothly attached and the low pressure was recovered as shown in Figure 9.

With such modifications, it was possible to convert part of the kinetic energy into pressure and therefore, a positive static pressure in the rear of the car is predicted. It can be noticed that the area of positive pressure in front of the car is larger than that at the exist in the rear of the car as a result of some losses. As mentioned earlier
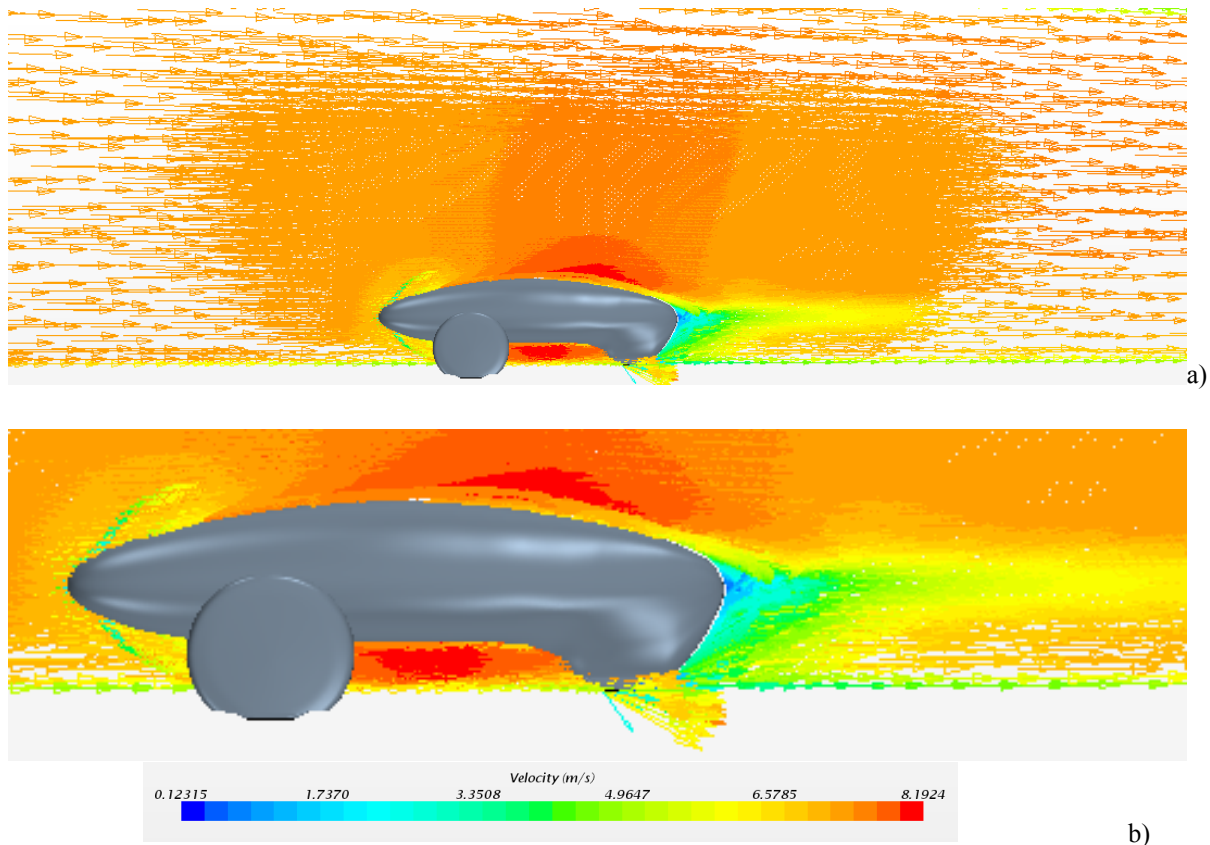
Figure 8. Spatial distribution of the velocity vector at flow stream velocity 7.3 m/s
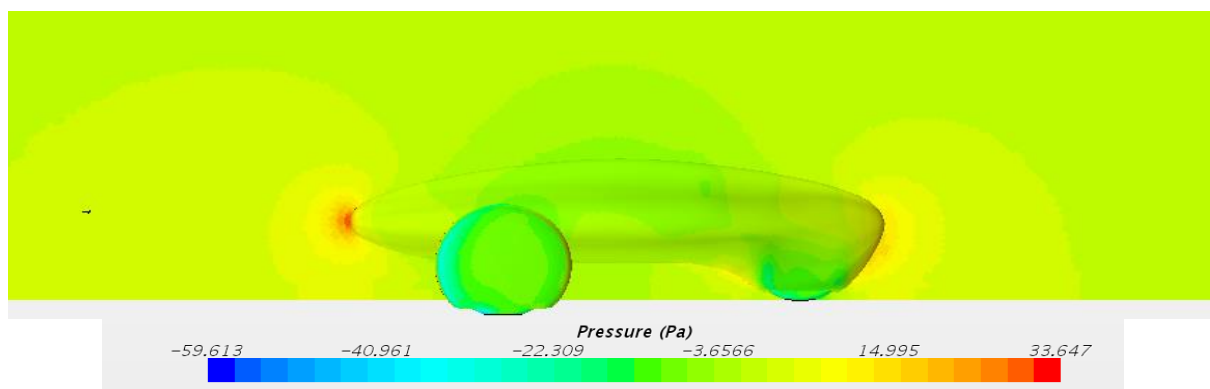
Figure 9. Spatial distribution of the pressure at flow stream velocity 7.3 m/s

the design iteration is not a straight forward process since any change in the car geometry is affecting the whole flow field whether it is upstream or downstream the car.

The static pressure distribution on the car surface is shown in Figure 10. The high pressure on front surfaces of wheel cover seem to have a significant contribution in the drag since the pressure cannot be recovered and wakes are expected to be formed behind the wheel. It is worth mentioning that the wheel of the car is assumed fixed in this study. Having a rotating wheel will shift the high pressure region a little up. With a smooth wheel cover or by having the wheel cover looks like a tear-drop shape may drop drag force further. As shown in the previous figure the body of the car shows recovering for the pressure at its rear part and therefore the pressure drag force is expected to be minimum and further improvement is not needed.

After examining the velocity vector and pressure distribution, it was important to look at the flow streamline around the car. The streamlines are generated from a small grid located in front of the car and forward integration is carried out. Figure 11 shows the smooth streamlines of the flow around the car without any obvious separation. The color of the streamlines shows a typical expected increase in the velocity as it passes on the top of the car surface. The airflow streamlines on the side of the car show also no evidence of flow separation on a large
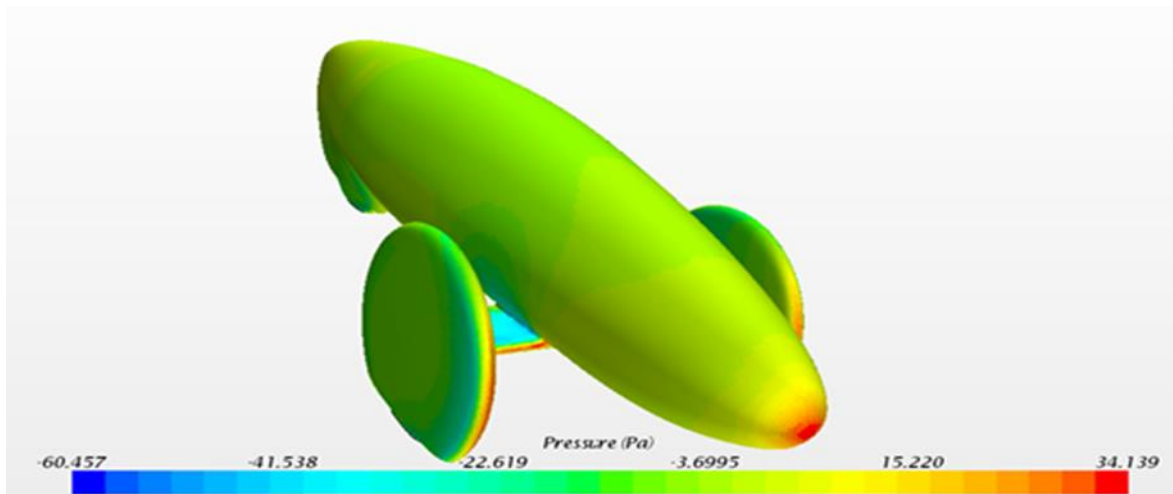
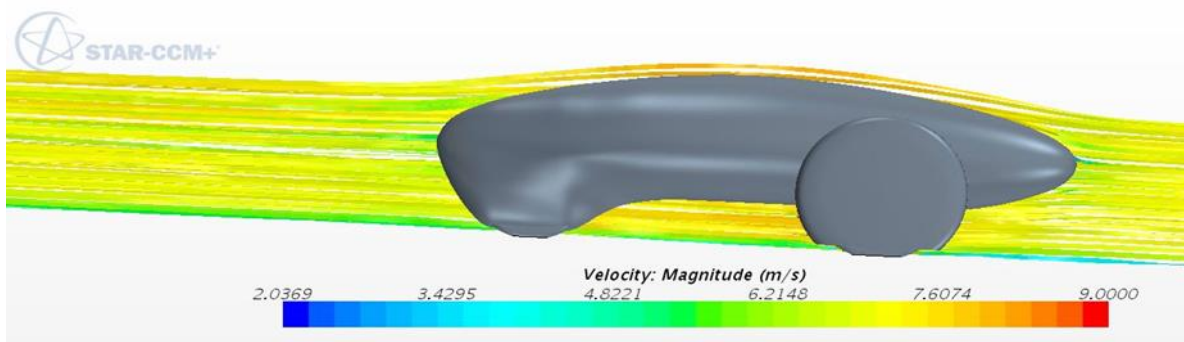**Figure 10.** Static pressure distribution on the surface of the final car design

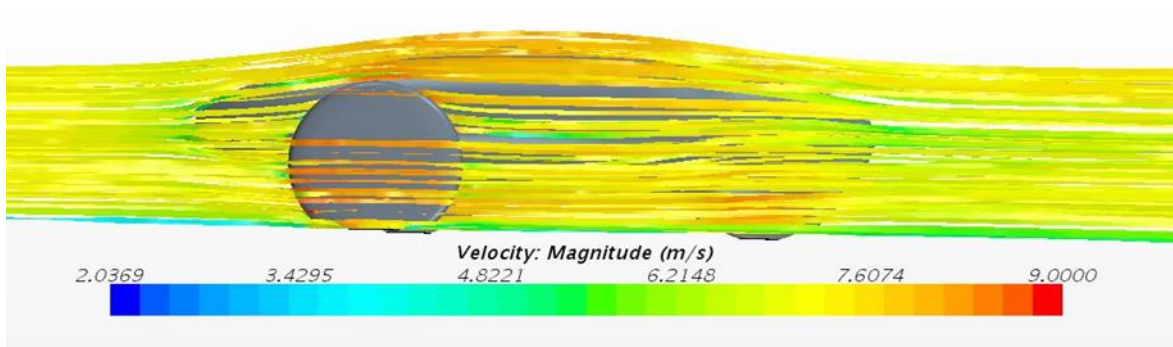**Figure 11.** Flow streamlines around the surface of final car design

Figure 12. Flow streamlines on the side surface of the car final design

scale. Nevertheless, it is expected to have wakes which could lead to small vortices behind the wheels but will not affect much the drag force due to their limited energy.

CONCLUSIONS

CFD simulations are carried out for Eco-Marathon car assuming steady isothermal incompressible flow with a non-rotating wheel. By modifying the front nose of the car to be longer, the underneath of the car to avoid the diffuser effect and the rear part of the car to recover the pressure, it was possible to achieve a drag coefficient of 0.127. The spatial distribution of the airflow velocity vectors and pressure around the car was enough to effectively modify the car shape to achieve a low drag force. In the final design, the air pressure on the wheel may

have significant contribution in the drag value and further improvement on the wheel cover may be needed to reduce that drag further. Mesh size was found to have approximately 2.3 % variation on the drag coefficient which is considered as part of the numerical error. The study was limited for a yaw angle zero and further study is needed to examine the flow for different value of yaw angle.

ACKNOWLEDGMENTS

REFERENCES

[1] Carello, M., Airale, A., Ferraris, A. and Messana, A., 2014. XAM 2.0: from Student Competition to Professional Challenge. Computer-Aided Design and Applications, 11(sup1), pp.561-567.

[2] Barnard, R.H., 2001. Road vehicle aerodynamic design-an introduction. Mechaero Publishing; 2nd Revised edition.

[3] Lu, W.F., Lim, H.W. and Goh, K.H., 2011, January. Engineering Design and Education: A Case Study on Designing A Competition Fuel Efficient Vehicle Through Experiential Learning. ASME 2011 International Design Engineering Technical Conferences and Computers and Information in Engineering Conference, pp. 741-750). American Society of Mechanical Engineers.

[4] Joseph Katz, 1995. Race Car Aerodynamics. Designing for Speed. Bentley Publishers.

[5] Abo-Serie, E., Sherif, M., Pompei, D., and Gaylard, A., 2014. CFD Simulation of External Distribution of Tail-Pipe Emissions Around a Stationary Vehicle Under Light Tail-Wind Conditions, SAE Technical Paper 2014-01-0586.

[6] Brunn, A., Wassen, E., Sperber, D., Nitsche, W. and Thiele, F., 2007. Active drag control for a generic car model. In Active Flow Control (pp. 247-259). Springer Berlin Heidelberg

[7] Bideaux E, Bobillier P, Fournier E, Gillieron P, El Hajem M, Champagne JY, Gilotte P, Kourta A. 2011. Drag Reduction by Pulsed Jets on Strongly Unstructured Wake: Towards The Square Back Control. Int J Aerodynamics,1(3/4):282–298.

[8] Heinemann T, Springer M, Lienhart H, Kniesburges S, Becker S., 2012. Active Flow Control on A 1:4 Car Model. Proceedings of the 16th Int. Symp. on Applications of Laser Techniques to Fluid Mechanics, Lisbon, Portugal.

[9] Wąsik, M. and Skarka, W., 2015. Influence of The Windscreens Inclination Angle on The Aerodynamic Drag Coefficient of The Cars Designed For The Race Shell Eco-Marathon Based on Numerical Simulations. Proceedings of The Institute of Vehicles 3(103).

[10] Danek, W., 2014. Determination of The Drag Coefficient High Performance Electric Vehicle. Modelowanie Inżynierskie, no. 21.

[11] Ahmed, E., Abo-Serie, E.. and Gaylard, A. , 2010. Mesh Optimization For Ground Vehicle Aerodynamics, Journal of CFD Letters, Vol. 2 No1.

[12] Eikeland, H. A., 2010. Aerodynamic Development and Construction of a Car for Participation in the Eco-Marathon Competition, EPT Master of Science in Product Design and Manufacturing, Norges Teknisk-Naturvitenskapelige University NTNU, Norway.

[13] Altinisik, A., Kutukceken, E. and Umur, H., 2015. Experimental and numerical aerodynamic analysis of a passenger car: Influence of the blockage ratio on drag coefficient. Journal of Fluids Engineering, 137(8), p.081104.

[14] Dumas, L., 2008. CFD-based optimization for automotive aerodynamics. In Optimization and Computational Fluid Dynamics (pp. 191-215). Springer Berlin Heidelberg.

[15] Lundberg, A., Hamlin, P., Shankar, D., Broniewicz, A. et al., "Automated Aerodynamic Vehicle Shape Optimization Using Neural Networks and Evolutionary Optimization," SAE Int. J. Passeng. Cars - Mech. Syst. 8(1):242-251, 2015, doi:10.4271/2015-01-1548.